

## Ion Propulsion System Design for the Comet Nucleus Sample Return Mission

John R. Brophy\*  
*Jet Propulsion Laboratory  
 California Institute of Technology  
 Pasadena, California*

Ion propulsion is now a legitimate option for deep space missions. One of the first science missions to use solar electric propulsion (SEP) may be the Comet Nucleus Sample Return (CNSR) mission which is designed to return samples of volatiles and dust from the nucleus of a comet. The use of SEP for CNSR makes the mission affordable and scientifically more attractive because it enables the use a smaller, lower cost launch vehicle and it significantly reduces the time required to return the samples to Earth. A detailed trade study was performed to identify the which ion engine and ion propulsion system technology improvements provide the greatest benefits to CNSR without introducing unacceptable technical risks. The trade study identified that the most attractive engine technology is an advanced version of the NSTAR engine characterized by an increase in specific impulse from 3100 seconds to 3800 seconds, a corresponding increase in the maximum engine power level from 2.3 kW to 3.1 kW and a doubling of the engine total impulse capability. This engine would be used in a four-engine system in which each engine is nominally operated at a maximum input power of 2.3 kW. In the event of an engine failure, however, the remaining three engines would be operated at up to 3.1 kW, enabling the propulsion system to be single fault tolerant without the need to add a fully redundant engine and its associated power processing unit. This advanced engine and system architecture are also shown to provide significant benefits to other deep-space missions of interest including Mars Sample Return, Neptune Orbiter, and missions to Saturn (Titan Explorer, Saturn Ring Observer).

### Introduction

After a development history spanning nearly forty years, the first use of solar electric propulsion (SEP) for primary propulsion on a deep-space mission began with the launch of the Deep Space 1 (DS1) spacecraft on October 28, 1998 [1]. This event marks a major milestone in the development of advanced propulsion for deep-space missions. The DS1 spacecraft uses a single-engine ion propulsion system (IPS), provided by the NASA Solar electric propulsion Technology Applications Readiness (NSTAR) project [2,3], as the primary on-board propulsion system. This propulsion system is designed to deliver a total  $\Delta V$  of 4.5 km/s to the 486-kg (initial wet mass) DS1 spacecraft while consuming only 81 kg of xenon.

Ion propulsion has now entered the mainstream of propulsion options available for deep-space missions. This is important because many of the deep-space missions that are relatively easy to perform from a

propulsion standpoint, such as planetary flybys, have already been accomplished. Future high priority mission classes, which include sample return missions and outer planet orbiters, place substantially greater demands on the capabilities of on-board propulsion systems. Ion propulsion can help make these missions affordable and scientifically more attractive by enabling the use of smaller, lower-cost launch vehicles and by reducing flight times.

Several scientifically interesting deep-space missions are now looking to the use of ion propulsion to significantly reduce total mission costs. These missions include Comet Nucleus Sample Return (CNSR), Venus Surface Sample Return (VSSR), Saturn Ring Observer, Titan Explorer, Neptune Orbiter, Europa Lander, and various Mars Sample Return options. Because these missions are more difficult, from a propulsion standpoint, than those used to justify the development of the NSTAR IPS technology, they benefit significantly from improvements to the ion propulsion technology that flew on DS1. Typically, the greatest overall benefit comes from increasing the total impulse capability per engine. As the engine total impulse capability is

---

\*NSTAR Project Manager, Member AIAA

increased, fewer engines are required for a given mission resulting in substantial savings in mass and cost. Additional savings may be obtained for some missions by increasing the maximum engine specific impulse, resulting in significant propellant mass savings.

This paper describes the results of a trade study that was performed to identify the best ion propulsion technology and system architecture to be developed in support of the CNSR mission. A key constraint was that the selected technology and architecture must also provide significant benefits to the other deep-space missions mentioned above.

All the technologies and system architectures considered in the trade study are derivatives of the single-engine, ion propulsion system developed by the NSTAR project for DS1. Therefore, before proceeding to the trade study a brief review of the NSTAR project and the validation of its technology is provided

#### **NSTAR Technology Validation**

The NSTAR project was initiated in 1992 and was designed to overcome the barriers preventing the use of solar electric propulsion on deep-space missions. To accomplish this the project had to achieve two major objectives:

1. Demonstrate that the NASA 30-cm diameter ion engine has sufficient life and total impulse capability to perform missions of near-term interest.
2. Demonstrate through a flight test that the ion propulsion system hardware and software could be flight qualified and successfully operated in space, and demonstrate control and navigation of an SEP-based spacecraft.

By all measures, these objectives have been met with unqualified success. Aside from an initial hiccup [2], the operation of the NSTAR ion propulsion system on DS1 has been flawless, and it successfully provided the  $\Delta V$  required for the July 29, 1999 flyby of the asteroid Braille. Consequently, ion propulsion is now a credible propulsion option for future deep-space missions. Complete details of how the NSTAR ion propulsion technology was validated for deep-space missions are given in the NSTAR Flight Validation Report [4], as well as in a shorter version of this report [5].

#### **NSTAR IPS Technical Description**

A simplified block diagram of the four major components of the NSTAR IPS is given in Fig. 1. The ion thruster uses xenon propellant delivered by the Xenon Feed System (XFS) and is powered by the Power Processing Unit (PPU), which converts power from the solar array to the currents and voltages required by the engine. The XFS and PPU are controlled by the Digital Control and Interface Unit (DCIU), which accepts and executes high-level commands from the spacecraft computer and provides propulsion subsystem telemetry to the spacecraft data system. To accommodate variations in the solar array output power with distance from the sun, the NSTAR IPS was designed to operate over a PPU input power range of 580 W to 2,500 W, with input voltages in the range 80 to 160 V. Discrete power levels within this range are referred to as "mission throttle levels". The mass of the NSTAR IPS as flown on DS1 is given in Table 1.

*Table 1 NSTAR IPS Component Masses*

<b>Component</b>	<b>Mass (kg)</b>
Ion Engine	8.33
Power Processing Unit (PPU)*	15.03
XFS minus Xenon Propellant Tank	12.81
Xenon Propellant Tank (for 81.5 kg of Xe)	7.66
Digital Control and Interface Unit (DCIU)	2.47
PPU to Ion Engine Cable	1.70
<b>Total</b>	<b>48.00</b>

\* Includes 1.7 kg for micrometeoroid shielding

#### **NSTAR Flight Validation**

One of the primary objectives of the NSTAR/DS1 flight validation activity is to verify that the system performs in space as it does on the ground. Key parameters of interest to future mission planners include the thrust and mass flow rate as a function of PPU input power and time. Two sets of performance tests of the ion propulsion system on DS1 have been performed, one at the beginning of the mission and the other after the engine had accumulated approximately 1800 hours of operation. The technique used to obtain direct thrust measurements on DS1 is described in Ref. 6. The results of these measurements are compared to pre-flight ground measurements and the NSTAR throttle table values in

Table 2. These data indicate that the engine thrust measured in space lies between the pre-flight thrust measurements and the end-of-life throttle table values. The data from Table 2 are also plotted in Fig. 2 as a function of the end-of-life PPU input power from the DS1 throttle table.

The performance of the xenon feed system on DS1 has been excellent. The mean value of the main flow and the two cathode flows are all within 1% of their respective planned flow rates [3].

In addition to performance, it is critically important to assess the extent to which the engine wear-out processes in space behave as they do in long-duration tests on the ground. Evaluation of key electrical parameters that influence engine life suggest that the engine erosion rates are probably not greater in space than they are on the ground. Indeed, these data [3] suggest that the ground test results are probably conservative.

Engine wear affects the engine performance, and since the thruster on DS1 can't be physically examined it is necessary to infer the wear from the measured performance. Ideally, the engine performance should be measured after it has processed a significant amount of propellant. A unique opportunity will exist to do this at the conclusion of what is now the DS1 science mission. Following the flyby of the Comet Borrelly in September 2001, the ion engine will have processed between 50 and 60 kg of xenon. This presents a unique opportunity to map the performance of an ion engine after it has accumulated by far been the longest-ever operating time in space. This opportunity will enable performance versus throughput comparisons with ground tests and will greatly improve our understanding of how well ground endurance tests reproduce actual in-space operation.

### **Comet Nucleus Sample Return (CNSR) Mission**

CNSR has been identified by the Solar System Exploration Subcommittee as the highest priority new mission for NASA's Exploration of the Solar System theme. This mission will return samples of volatiles and dust from the nucleus of a comet, and will provide new insight into our origins, evolution, and destiny. Advanced solar electric propulsion enables a total mission duration of 6 to 10 years, as well as the use of a smaller, much less expensive launch vehicle. The use of ion propulsion for CNSR enables *both* a

much shorter trip time *and* a smaller launch vehicle than a spacecraft using a bi-propellant on-board propulsion system

### **CNSR SEP Trade Study**

The CNSR mission may be the first flagship science mission to use ion propulsion. The Deep Space 1 mission was designed to demonstrate new technologies, with collection of science data only a secondary consideration. In contrast, science missions require that the bus subsystems (including on-board propulsion) have higher reliabilities. Specifically, CNSR and other deep-space science missions will require that the ion propulsion systems be single-fault tolerant.

A trade study, using Brooks 2 as the target comet, was conducted to determine which engine and system technology improvements to the basic NSTAR technology provide the greatest mission benefits for CNSR without introducing unacceptable technical risk. Five different engine technologies, as identified in Table 3, were considered. These technologies range from the basic NSTAR engine (Engine Option 1) to a 5-kW NSTAR-derivative engine (Engine Option 5). These options are characterized by differences in three major parameters: the maximum engine input power, the maximum specific impulse, and the engine total impulse (or throughput) capability.

In addition, seven different single-fault-tolerant system configurations were considered. These systems, listed in Table 4, are briefly summarized below. System Option:

1. A conventional system architecture consisting of four engine-PPU strings identical to the single string which flew on DS1. A maximum of three engines is operated simultaneously at 2.3 kW each. The fourth string is included to meet the single-fault tolerant requirement.
2. A conventional system architecture consisting of five engine-PPU strings identical to the single string which flew on DS1. A maximum of four engines is operated simultaneously at 2.3 kW each. The fifth string is included to meet the single-fault tolerant requirement.
3. A conventional system architecture consisting of four engine-PPU strings with upgraded engines and PPU's. A maximum of four engines is operated simultaneously at 2.3 kW each. Single-fault tolerance is obtained by operating the remaining three engine-PPU strings at 133% of

their nominal power of 2.3 kW in the event of an engine or PPU failure early in the mission.

4. An unconventional system architecture consisting of four upgraded engines and a single, internally-redundant High-Voltage/Neutralizer Assembly (HVNA) which provides the high voltage and neutralizer power supply functions for all four engines, a central neutralizer cathode assembly, and four separate discharge power supply boxes. A maximum of four engines is operated simultaneously at 2.3 kW each. Single-fault tolerance is obtained by operating the remaining three engines at 133% of their nominal power of 2.3 kW in the event of an engine or PPU failure early in the mission.
5. A conventional system architecture consisting of three engine-PPU strings with upgraded engines and PPU's. A maximum of three engines is operated simultaneously at 3.1 kW each. Single-fault tolerance is obtained by operating the remaining two engine-PPU strings at 150% of their nominal power of 3.1 kW in the event of an engine or PPU failure early in the mission.
6. An unconventional system architecture consisting of three upgraded engines and a single, internally-redundant High-Voltage/Neutralizer Assembly (HVNA) which provides the high voltage and neutralizer power supply functions for all three engines, a central neutralizer cathode assembly, and four separate discharge power supply boxes. A maximum of three engines is operated simultaneously. Single-fault tolerance is obtained by operating the remaining two engines at 150% of their nominal power of 3.1 kW in the event of an engine or PPU failure early in the mission.
7. A conventional system architecture consisting of three 5-kW engine-PPU strings. A maximum of two engines is operated simultaneously at 4.6 kW each. The third string is included to meet the single-fault tolerant requirement.

System Option 1 is assumed to use an NSTAR-like xenon feed system (XFS). All of the other system options are assumed to use an advanced XFS based on the availability of new flow system components. For each system it was assumed that the maximum input power available to the propulsion system is 10 kW. System configurations 2, 3 and 4 are shown in block-diagram form in Fig. 3.

For the purposes of the trade study the target comet Brooks 2 was selected. Other target comets were examined to make sure that the use of Brooks 2

did not artificially impact the IPS technology selection. This survey indicated that Brooks 2 appears to be relatively representative of the short-period comets that are candidates for CNSR.

The impact of the engine technology options listed in Table 3 on the initial CNSR spacecraft dry mass is given in Fig. 4 as a function of solar array power assuming the target comet is Brooks 2 and the launch vehicle is a Delta IV medium. The solar array power is specified by the beginning of life (BOL) power at 1 AU from the sun. The initial spacecraft dry mass includes the mass of the IPS. For these trajectory calculations the launch vehicle is assumed to take the spacecraft to Earth escape with a slightly positive hyperbolic excess energy. The trajectory is optimized the value of this energy and the operation of the SEP system to maximize the burnout mass. A mass of 300 kg is assumed to be left at the comet, and the SEP system is used for transportation both to and from the comet.

The performance of engine option 2 is not shown in Fig.4, but is similar to Engine Option 1. The performance of Engine Options 3, 4 and 5 are all very similar, even though Option 3 has a lower specific impulse. All three of these options provide approximately a 40-kg increase in spacecraft dry mass relative to engine option 1. This is significant because the total mass of the CNSR payload is roughly 250 kg. So 40 kg represents about 16% of the payload mass.

Two variations of Engine Option 4 are given in Fig. 4. One variation corresponds to the use of a conventional NSTAR neutralizer cathode, and the other to the use of a new, low-flow neutralizer cathode. These data suggest that the use of a low-flow neutralizer cathode provides a benefit of approximately 10 kg in spacecraft dry mass.

For a 17-kW, BOL at 1AU solar array, the power available to the propulsion system as a function of mission time is given in Fig. 5. These data assume that the rest of the spacecraft requires a power level of 450 W. The available power decreases rapidly at the beginning of the mission as the spacecraft gets farther from the sun. For the first 135 days of the mission the solar array can provide more power than the 10-kW maximum that the propulsion system can process. Although this power is wasted it does not have a strong impact on the mission performance since the power decreases so rapidly. The excess power is the result of the solar array being sized for other phases in

the mission rather than for the beginning of the mission.

The data in Fig. 5 indicate that for most of the mission the available power is significantly below 10 kW, however, at the end of the mission, the available power increases back to 10 kW as the return trajectory takes the spacecraft back to 1 AU. Radiation degradation of the solar array accounts for the difference between beginning and end of life power levels.

The engine input power as a function of mission time is given in Fig. 6 assuming 4, 3 or 2 functioning engines. With 4 functioning engines, the maximum engine input power is 2.3 kW, with 3 engines it is 3.1 kW and with only 2 functioning engines the maximum engine input power is 4.6 kW. When the engine input power is zero, the propulsion system is off and the spacecraft is coasting. In each case, the spacecraft arrives at the comet after 1100 days and departs from the comet approximately 100 days later (mission time 1200 days). For the transfer to the comet, the engine input power never drops below approximately 1.5 kW (with one exception for the 2-engine case). For the return trip, the engines must be throttled to their minimum input power levels. This dictates a large dynamic range requirement for the thrusters. Finally, Fig. 6 indicates that both the 2.3-kW and 3.1-kW thrusters must be operated at full power at the end of the mission. This places a requirement on the xenon feed system to be able to supply the full-power flow rate to the thruster when the xenon storage pressure is a minimum.

The effect of the thruster maximum specific impulse on the total propellant required is given in Fig. 7. Increasing the  $I_{sp}$  from 3100 seconds to 3800 seconds reduces the amount of xenon required by 125 kg. This propellant reduction is more than the original NSTAR engine design throughput capability. Therefore, increasing the engine  $I_{sp}$  may reduce the number of engines required to process the total propellant load, provided the engine throughput capability does not decrease significantly as a result of operating at a higher specific impulse.

### **Trade Study Results**

The ion propulsion system dry mass is given in Fig. 7 for selected combinations of engine and system architectures. The pair of numbers below each bar in Fig. 7 represent the engine option and the system option from Tables 3 and 4, respectively. These data indicate, as expected, that the low-tech systems

(represented by the lower numbered options) have a higher dry mass than the more advanced technology options. The lightest system dry mass is obtained with the use of the most new technologies as represented by the (thruster, system) combination (5,6). This combination assumes the development of a 5-kW, very-high-throughput engine along with the development of the system architecture given in Fig. 3c (with 3 engines instead of 4). This system is nearly 60 kg lighter than the conventional system represented by (1,2), but this mass savings comes with a considerable cost and development schedule risk. The mass of the xenon propellant tanks are not included in the IPS mass values given in Fig. 7, so the higher  $I_{sp}$  systems would actually show a greater mass benefit than is indicated in this figure.

Subtracting the IPS dry mass from the initial spacecraft dry mass from Fig. 4 for a 17-kW (BOL at 1 AU) solar array results in the net spacecraft masses given in Fig. 8 for selected engine and system technology options. The net spacecraft dry mass is defined as the spacecraft dry mass minus the dry mass of the ion propulsion system. Therefore, the net spacecraft mass is everything on the spacecraft that isn't propellant or part of the ion propulsion system. For the data in Fig. 8 the mass of the solar array is included in the net spacecraft mass because the solar array is used to power the payload at the comet. Even though the solar array is very large, the spacecraft operations at the comet will take place when the comet distance from the sun is approximately 3 AU or greater, so that all of the available solar array power will be needed.

The goal of the ion propulsion system trade study is to maximize the net spacecraft mass without introducing unacceptably large technical and schedule risks. The data in Fig. 8 indicate that the largest net spacecraft masses are obtained by the development of either a 5-kW engine and/or the development of the new system architecture given in Fig. 3c. The collective ion propulsion expertise at the Glenn Research Center and JPL concluded that both of these developments incurred too great a technical and schedule risk for near-term, deep-space science missions.

This leaves the only remaining system options as 1, 2 or 3. From Fig. 8 it is clear that system option 3 provides a significant mass benefit relative to options 1 or 2, especially when coupled to Engine Options 3 or 4. The (Engine Option, System Option) combinations of (3,3) and (4,3) result in nearly

identical net spacecraft masses. Therefore, selection between these cases must be based on which engine option has the lowest development risk.

The required engine throughput capability is given in Fig. 9 for all five engine options. The higher  $I_{sp}$  of Engine Option 4 results in a significantly lower propellant throughput requirement than Options 2 or 3. Engine Option 5 (the 5-kW engine) has the same  $I_{sp}$  as Engine Option 4, but the system configurations that use the 5-kW engine have fewer engines resulting in a much greater throughput requirement per engine. The throughput requirement for engine option 1 given in Fig. 9 assumes the system architecture option 2. For engine options 2, 3, and 4 the systems are assumed to include a total of 4 engines. If one engine fails at the beginning of the mission the remaining engines must be capable of processing the total propellant loading with a maximum input power of 3.1 kW per engine.

The throttling envelopes for engines 1, 3 and 4 are given in Fig. 10. Operation at 3.1 kW for engine option 3 is accomplished by increasing both the beam voltage (specific impulse) and the beam current relative to Option 1 (the NSTAR baseline). The  $I_{sp}$  is increased from 3100 s to 3500 s by increasing the beam voltage from 1100 V to 1250 V and the maximum beam current from 1.76 A to 2.07 A. Increasing net accelerating voltage is straightforward and there is believed to be little risk of introducing unknown failure modes is doing so. Increasing the beam current, requires an increase in discharge current which carries a greater risk of introducing new failure modes associated with cathode life.

On the other hand, operation at 3.1 kW for Engine Option 4 requires only an increase in the beam voltage from 1100 V to 1500 V. In this option the maximum beam current never exceeds that demonstrated in the long-duration life tests performed under the NSTAR project. Since these tests are time consuming, expensive and essential for user acceptance, it is critical that the selected engine technology not invalidate the extensive life testing performed to date. The higher beam voltage requires a modification to the beam power supply in the NSTAR PPU. This power supply is made up of four 300-V modules connected in series. The addition of a fifth module would produce the desired output voltage with a minimum technical risk.

The combination of lower required throughput and lower risk of introducing new failure modes resulted in the selection of Engine Option 4 as the

preferred option. The end result of the trade study, then was the selection of Engine Option 4 and System Option 3. This combination (4,3) provides the greatest system mass benefits at the lowest development risk.

### **Other Deep-Space Missions**

A comparison of systems based on NSTAR technology, the Advanced NSTAR technology selected above, and the 5-kW NSTAR derivative technology are compared in Table 5 for the CNSR mission, a Mars Sample Return option, the Neptune Orbiter mission, and missions to Saturn (Titan Explorer and Saturn Ring Observer).

For the NSTAR columns in this table, the engine was assumed to have only its design throughput capability of 88 kg. This assumption results in the need for many engines to process the total xenon propellant load. The number of engines needed to process the total propellant load is given in Fig. 11 as a function of the engine throughput capability for the above four missions. It is clear that increasing the engine throughput to between 170 and 195 kg greatly reduces the number of engines required for these missions. By increasing the engine throughput capability by approximately 100 kg (from 88 kg to 190 kg), the number of engines required for these missions decreases by 3 to 5. But, to reduce the number of engines by one more requires another 60- to 100-kg increase in the throughput capability. Thus, there is a diminishing return for increasing the engine throughput capability beyond 200 kg for deep-space missions with the power levels assumed herein.

Finally, Table 5 indicates that the 5-kW engine based systems save only 1 or 2 engines and 1 PPU relative to the "Advanced NSTAR" system selected by the trade study. In addition, the 2-engine savings is only realized if the throughput capability of the 5-kW engine is greater than 330 kg. Thus a successful 5-kW engine development program would have to produce an engine with twice the maximum input power capability of the DS1 NSTAR engine and nearly four times its throughput.

### **NSTAR Engine Throughput Capability**

The results of the CNSR trade study and the examination of Advanced NSTAR systems for other deep-space missions of interest strongly indicate that the engine throughput capability is one of the most

important engine and system performance parameters. Establishing the throughput capability of the NSTAR ion engine has always been one of the principal goals of the NSTAR project. An extensive ground test program, together with detailed analyses of the critical wearout modes and the flight test on DS1, is being used to validate the ion engine service life. Three long-duration ground tests have been performed which processed 10, 21, and 88 kg of xenon (corresponding to 1,000 hrs, 2,000 hrs, and 8,200 hrs of operation at full power, respectively). In addition, a fourth on-going test, called the extended life test (ELT) has so far processed 100 kg of xenon after more than 11,000 hours of operation. This test is on schedule to demonstrate an engine throughput of 125 kg by the end of the year 2000. These tests were designed to identify unknown failure modes, characterize the parameters which drive known failure mechanisms and determine the effect of engine wear on performance.

Detailed analyses and long-duration test data have been presented in numerous papers [8,9,10,11]. A summary of what is known about the NSTAR engine throughput capability was presented to an independent review board which concluded that the NSTAR ion engine could process a total propellant throughput of 130 kg with a low wear-out failure risk with one caveat [12]. This caveat was that the average engine power level must be less than 2.1 kW. Operation at the full power point of 2.3 kW is allowed, but not for the full 130-kg throughput. This restriction was imposed in order to obtain at least a factor of two margin on all known failure modes. Most out-bound deep-space missions that would use solar electric ion propulsion tend to meet this requirement automatically since the available power decreases with increasing solar range.

The extensive life testing performed by under the NSTAR project has identified electron-backstreaming as one of the key engine wear-out failure modes. The on-going ELT using the DS1 flight spare ion engine has provided additional information regarding electron-backstreaming allowing the analysis of this failure mode to be updated from a previous paper [11].

During normal engine operation the outer electrode of the ion accelerator system (called the accelerator grid) is biased sufficiently negative of the ambient space plasma potential to prevent electrons in the ion beam from "backstreaming" into the positive high voltage engine. As the accelerator grid wears

during operation the apertures in the grid enlarge due to ion sputtering, and more negative voltage is required to prevent electron backstreaming. If the voltage required to prevent electron backstreaming is more negative than can be supplied by the accelerator grid power supply the engine has failed.

The variation in the accelerator grid voltage at which electron-backstreaming begins is given in Fig. 12 for both the 8,200-hr Long Duration Test (LDT) and the on-going ELT. The variation in electron-backstreaming onset voltage is approximately a linear function of time during the LDT. The step function changes evident in electron-backstreaming voltage from the ELT correspond to intentional changes in thrust level during the test.

The solid lines correspond to a semi-empirical model developed to predict the variation in electron-backstreaming voltage with time. This model is described in more detail in Ref. 11. A slight modification to the model of Ref. 11 was made to better fit the data observed through the first 2,000 hours of both tests. This change deals with how the "cusp" on the hole wall is eroded. The process which forms the accelerator grid apertures is a 50/50 chemical etch which leaves a "cusp" of material as indicated in Fig. 13. This cusp affects the measured hole diameter, but has a lesser impact on electron-backstreaming. The solid lines in Fig. 12 were obtained by assuming that the volume of material contained within the cusp is "morphed" into a cylindrical hole wall geometry at the beginning of life, with the diameter of the new hole such that the total amount of material is unchanged. The diameter of the resulting new hole then assumed to increase uniformly across the grid thickness as the grid wears.

The model is semi-empirical in that the maximum material removal rate in the accelerator grid apertures could not be specified a priori. Instead, the erosion rate was calculated from the post-LDT measurements of the accelerator grid apertures. This material removal rate was then assumed to be constant over the LDT and was assumed to be the same for the ELT for operation a full power. For operation a throttled conditions during the ELT this material removal rate was scaled with accelerator grid current and ion beam flatness parameter.

In addition, the model requires as an input the separation distance between the grids during operation. The electron-backstreaming onset voltage is extremely sensitive to the grid separation and this distance cannot be specified with sufficient accuracy

a priori. Therefore, the value for the grid separation is selected to provide obtain the best fit with the experimental data. For the LDT data in Fig. 12 this distance is 0.660 mm, and for the ELT it is 0.620 mm. It turns out the measuring the electron-backstreaming voltage is a very sensitive way to measure the effective screen-accelerator grid separation distance.

Using a numerical model and software developed by K. Ishihara and Y. Arakawa of the University of Tokyo, the variation of electron-backstreaming voltage with accelerator grid hole diameter and grid separation given in Fig. 14 is calculated for operation at the NSTAR full power point. These calculations cover the range of hole diameters, grid separations and accelerator grid voltages applicable to the NSTAR thruster operating at full power over its complete service life.

Approximating the variation in electron-backstreaming voltage with grid separation for a fixed hole diameter as linear function, and using the curve fits from Fig. 14, allows the accelerator grid voltage at which electron-backstreaming begins to be written as,

$$V_a = (-171.4I_g + 281.1)d_a - 61.1 \quad (1)$$

where  $I_g$  is the grid separation in millimeters,  $d_a$  is the accelerator hole diameter also in millimeters. Rewriting this equation gives the accelerator grid hole diameter at which electron-backstreaming begins for a given accelerator grid voltage,  $V_a$  and screen-accelerator grid separation,

$$d_a = \frac{V_a + 61.11}{-171.1I_g + 281.1} \quad (2)$$

From Ref. [11] the time,  $T$ , to erode the accelerator grid apertures to a diameter  $D$  is given as,

$$T = (d_a^2 - d_0^2) \left( \frac{\pi \rho t_a e f_a N_h}{4 J_b \alpha_a Y m_g (1 - \beta) \lambda_h} \right) \quad (3)$$

where  $\rho$  is the density of the grid material,  $t_a$  is the thickness of the accelerator grid,  $e$  is the electron charge,  $f_h$  is the flatness parameter governing material removal from the accelerator grid hole walls,  $N_h$  is the number of holes in the accelerator grid,  $J_b$  is the ion beam current,  $\alpha_a$  is the ratio of accelerator grid

current to beam current,  $Y$  is the sputter yield for xenon ions striking the grid material at an energy approximately equal to the accelerator grid voltage,  $m_g$  is the mass of an atom of grid material,  $\beta$  is the fraction of the ion current striking the accelerator grid the hits on the downstream face of the grid, and  $\lambda_h$  is a parameter which corrects the sputter yield for the actual incident ion energy and angle. The parameter,  $d_0$  in Eq. (3) corresponds to the effective hole diameter that results from “morphing” the cusp material into a straight-walled cylindrical hole. For the NSTAR accelerator grid  $d_0 = 1.205$  mm.

The combination of parameters,  $(1-\beta)\lambda_h$ , determines the erosion rate of the accelerator hole walls. It is this combination that was selected in the semi-empirical model given in Fig. 12 to match the erosion rate measured observed during the LDT. To achieve this match requires that

$$(1-\beta)\lambda_h = 0.11 \quad (4)$$

Combining Eqs. (2), (3) and (4) and using the result in the probabilistic framework described in Ref. [11] allows the failure probability due to electron-backstreaming to be calculated. The value for the flatness parameter governing hole wall erosion can be determined from the accelerator grid hole diameters measured before and after the LDT. Using these data, as given in Ref. [9], allows the mass lost from the holes to be calculated as a function of radial position on the grid as shown in Fig. 15. Integrating the curve fit to these data results in a value for the flatness parameter of,  $f_h = 0.28$ .

Finally, using Eqs. (2) and (3) in a Monte Carlo simulation with the values of the parameters  $\rho$ ,  $t_a$ ,  $N_h$ ,  $J_b$ ,  $\alpha_a$ ,  $Y$ , and  $m_g$  given in Ref. [11], the failure probability due to electron-backstreaming can be calculated. The results of this process are given in Fig. 16 for operation at the NSTAR full-power point with three different approaches for changing the accelerator grid voltage as the grid wears. In the first case the accelerator grid voltage is fixed at  $-250$  V. This results in the lowest throughput capability because it has the highest average grid erosion rate. The second case maintains the accelerator grid voltage at  $-180$  V until the electron-backstreaming voltage margin is reduced to  $10$  V, then the accelerator grid voltage is decreases to  $-250$  V for the rest of the engine life. This approach provides a significant increase in engine throughput capability

for this wear-out mode relative to fixing the accelerator grid voltage at  $-250$  V. The third case also maintains the accelerator grid voltage at  $-180$  V until the electron-backstreaming voltage margin is reduced to 10 V, at this point, however, the accelerator grid voltage is decreased in 10 V increments every time the electron-backstreaming voltage margin is 10 V, until an accelerator grid voltage of  $-250$  V is reached. This approach provides only a slight benefit relative to the single step used in the second case.

For the second case approach the engine throughput capability for the electron-backstreaming failure mode is greater than 210 kg.

### **Acknowledgements**

The author acknowledges the work of the CNSR IPS trade study participants including Ray Becker, Gani Ganapathi, Charles Garner, Kurt Hack, John Hamley, Don Nieraeth, Steve Oleson, Michael Patterson, Jay Polk, Vince Rawlin, Jon Sims, Jim Sovey, and Jeff Weiss. The author also acknowledges the major contributions of all the NSTAR Project members to making ion propulsion a legitimate propulsion for deep space missions. The work described in this paper was conducted, in part, by the Jet Propulsion Laboratory, California Institute of Technology, under contract to the National Aeronautics and Space Administration.

### **Conclusions**

Most of the future deep space science missions of near-term interest are planning the use of solar electric propulsion based on derivatives of the NSTAR ion propulsion system that flew on Deep Space 1 in order to reduce mission costs and trip times. These missions include CNSR, MSR, VSSR, Titan Explorer, Saturn Ring Observer, and Neptune Orbiter. A detailed trade study performed in support of the CNSR advanced mission study activity identified the improvements to the NSTAR technology which provide the greatest mission benefits for the lowest added technical risk. These improvements include increasing the maximum engine specific impulse to 3800 seconds, increasing the maximum engine input power to

3.1 kW, and increasing the engine propellant throughput capability to 195 kg.

### **References**

1. Rayman, M. D., "Results from the Deep Space 1 Technology Validation Mission," IAA-99-IAA.11.2.01, presented at the 50<sup>th</sup> International Astronautical Congress, 4-8 Oct 1999, Amsterdam, The Netherlands.
2. Polk, J. E., et al., "In-Flight Performance of the NSTAR Ion Thruster Technology on the Deep Space One Mission," AIAA-99-2274, presented at the 35<sup>th</sup> AIAA/ASME/SAE/ASII Joint Propulsion Conference, June 21-23, 1999.
3. Sovey, J. S., et al., "Development of an Ion Thruster and Power Processor for New Millennium's Deep Space 1 Mission," AIAA-87-2776, presented at the 33<sup>rd</sup> Joint Propulsion Conference, Seattle, WA, July 1997.
4. Kakuda, R., "NSTAR Flight Validation Report," MOR-602, JPL D-18219, internal document, November 1, 1999.
5. Brophy, J. R., et al., "Ion Propulsion," internal JPL document, presented at the Deep Space 1 Technology Validation Symposium, February 2000.
6. McElrath, T. P., Dongsuk, HAN, and Ryne, M. S., "Radio Navigation of Deep Space 1 During Ion Propulsion Stage Usage."
7. Ganapathi, G. B. and Engelbrecht, C. S., "Post-Launch Performance Characterization of the Xenon Feed System on Deep Space One," AIAA-99-2273, presented at the 35<sup>th</sup> AIAA/ASME/SAE/ASEE Joint Propulsion Conference, June 21-23, 1999.
8. J. E. Polk, et al., "The Effect of Engine Wear on Performance in the NSTAR 8,000-Hour Ion Engine Endurance Test," AIAA-97-3387, presented at the 33<sup>rd</sup> AIAA/ASME/SAE/ASEE Joint Propulsion Conference, July 1997.
9. J. E. Polk, et al., "An Overview of the Results from an 8,200-Hour Wear Test of the NSTAR Ion Thruster, AIAA-99-2446, presented at the 35<sup>th</sup> AIAA/ASME/SAE/ASEE Joint Propulsion Conference, Los Angeles, CA, June 1999.
10. Anderson, J. R., et al., "Results of an Ongoing Long Duration Ground Test of the DS1 Flight Spare Engine," AIAA-99-2875, presented at the

35<sup>th</sup> AIAA/ASME/SAE/ASEE Joint Propulsion Conference, Los Angeles, CA, June 1999.

11. Brophy, J. R., et al., "The Ion Propulsion System on NASA's Space Technology 4/Champollion Comet Rendezvous Mission," AIAA-99-2856, presented at the 35<sup>th</sup> AIAA/ASME/SAE/ASEE Joint Propulsion Conference, Los Angeles, CA, June 1999.
12. Parker, G., "NSTAR Risk Assessment for Discovery Proposals," Interoffice Memorandum PFPO-GLP-2000-002, April 5, 2000, internal JPL document.

**Table 2 Comparison of Flight Thrust Measurements to the Throttle Table Values**

DS1 Throttle Table		DS1 Throttle Table Thrust (mN)	Pre-Flight Functional Test (mN)	DS1 Beginning of Life Thrust (mN)	DS1 after 1800 hrs of Thrusting Thrust (mN)
Mission Throttle Level	PPU EOL Input Power (kW)				
6	0.577	20.69	20.87	20.80 ± 0.13	20.71 ± 0.082
13	0.729	24.55			24.23 ± 0.065
20	0.825	27.47			26.99 ± 0.073
27	0.994	32.12		31.77 ± 0.21	31.46 ± 0.074
34	1.111	37.35	34.94		36.62 ± 0.231
48	1.345	47.87		47.30 ± 0.14	
62	1.579	57.90	55.69		
69	1.712	63.17		62.23 ± 0.41	
76	1.863	68.37	66.00		
83	2.006	73.60		72.56 ± 0.41	
90	2.137	78.39		77.39 ± 0.45	
111	2.567	92.67	91.70		
111	2.567	92.67	93.06		

**Table 3 Trade Study Engine Options**

Engine Option	Description	Max. Isp (s)	Max. Engine Input Power (kW)	Max. PPU Input Power (kW)
1	NSTAR	3100	2.3	2.5
2	Low-Isp Advanced NSTAR	3100	3.1	3.4
3	Med.-Isp Advanced NSTAR	3500	3.1	3.4
4	High-Isp Advanced NSTAR	3800	3.1	3.4
5	5-kW NSTAR Derivative	3800	4.6	5.0

**Table 4 Trade Study System Options**

System Option	Architecture Description	Number of Engines	Number of PPU's	Maximum number of engines operating simultaneously	Nominal Maximum Engine Input Power (kW)	Contingency Maximum Engine Input Power (kW)
1	Conventional one engine per PPU with spare thruster/PPU string to be single-fault-tolerant	4	4	3	2.3	2.3
2	Conventional one engine per PPU with spare thruster/PPU string to be single-fault-tolerant	5	5	4	2.3	2.3
3	Conventional one engine per PPU, operate remaining thruster/PPU strings at 133% of nominal power in the event of a fault	4	4	4	2.3	3.1
4	Single internally redundant High Voltage and Neutralizer Assembly, operate remaining thruster/PPU strings at 133% of nominal power in the event of a fault	4	1*	4	2.3	3.1
5	Conventional one engine per PPU, operate remaining thruster/PPU strings at 150% of nominal power in the event of a fault	3	3	3	3.1	4.6
6	Single internally redundant High Voltage and Neutralizer Assembly, operate remaining thruster/PPU strings at 150% of nominal power in the event of a fault	3	1*	3	3.1	4.6
7	Conventional one engine per PPU with spare thruster/PPU string to be single-fault-tolerant	3	3	2	4.6	4.6

\*Also requires a separate discharge power supply for each engine

**Table 5 IPS Technology Options for Deep-Space Missions**

	CNSR			Mars Sample Return			Neptune Orbiter			Titan Explorer		
		Advanced			Advanced			Advanced		Advanced		
	NSTAR	NSTAR	5-kW	NSTAR	NSTAR	5-kW	NSTAR	NSTAR	5-kW	NSTAR	NSTAR	5-kW
Max. IPS Input Power (kW)	10	10	10	10	10	10	10	10	10	10	10	10
Solar Array Size, BOL at 1 AU (kW)	17	17	17	17	17	17	21	21	21	17	17	17
Minimum number of engines required to process the available power	4	3	2	4	3	2	4	3	2	4	3	2
Total Xenon Propellant Load (kg)	658	530	548	---	777	---	837	680	678	639	567	560
Number of engines required to process the available propellant	8	3	2	---	4	---	10	4	2	8	3	2
Required throughput per engine (kg)	82	177	274	---	194	---	84	170	339	80	189	280
Number of engines required to make the system single fault tolerant	9	4	3	---	5	---	11	5	3	9	4	3
Number of PPU's required to make the system single fault tolerant	5	4	3	---	4	---	5	4	3	5	4	3

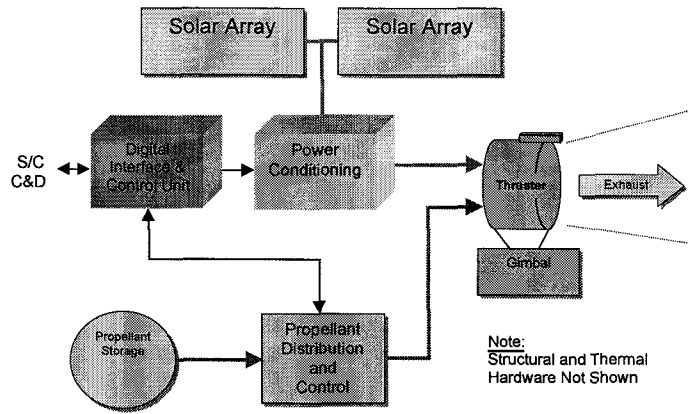


**Fig. 1 Single-string ion propulsion block diagram**

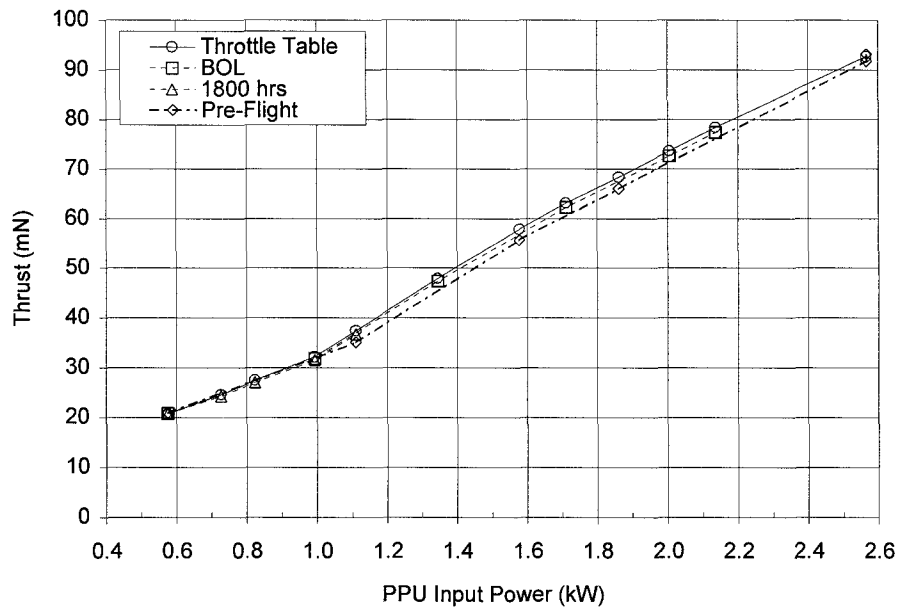
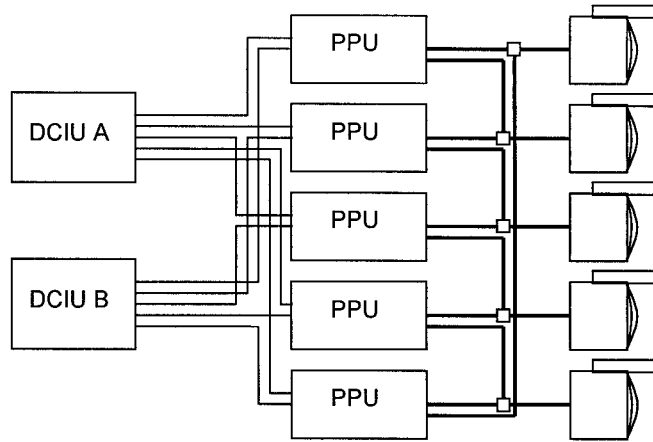
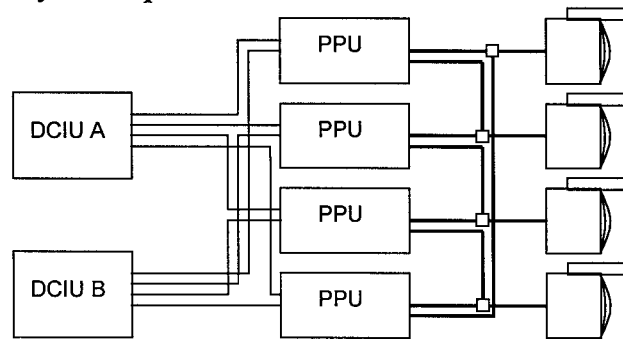


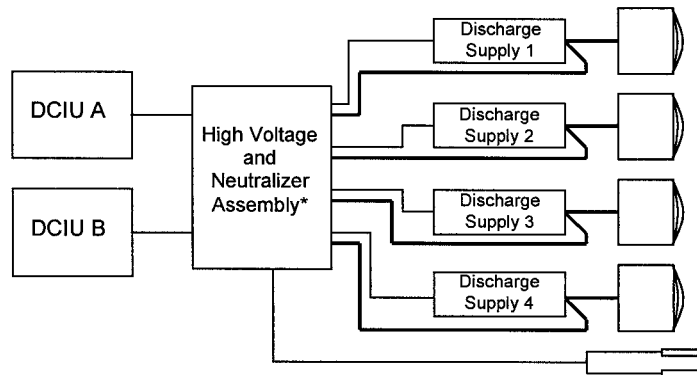
**Fig. 2 Thrust measured in-flight compared to the pre-flight measurements and the throttle table values.**



*a) System Option 2*



*b) System Option 3*



*c) System Option 4*

**Fig. 3 Ion propulsion system configuration options.**

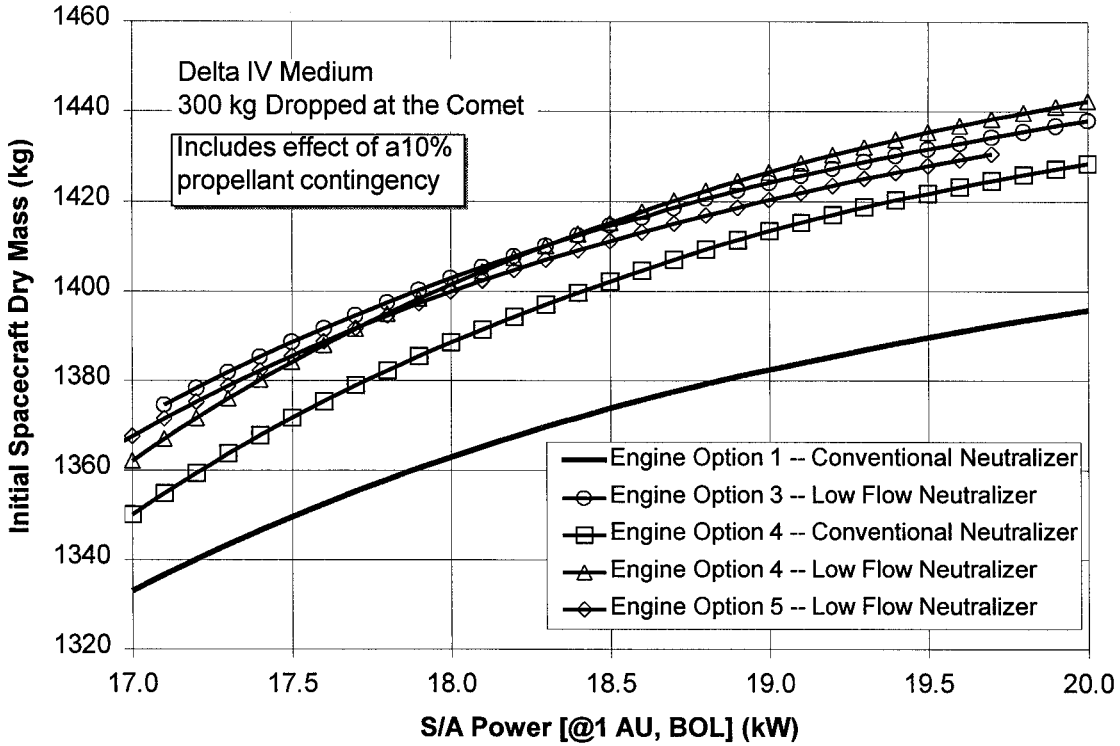


**Fig. 4. Effect of engine technology on spacecraft dry mass for comet Brooks 2.**

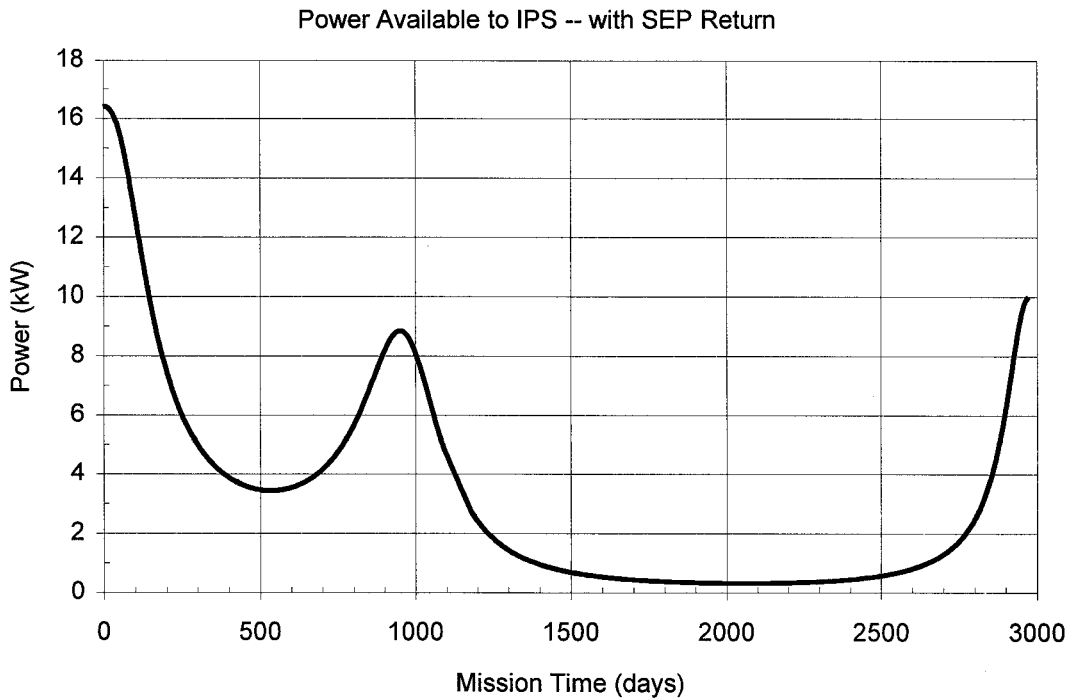


**Fig. 5 Power available to the IPS as a function of time during the CNSR mission.**

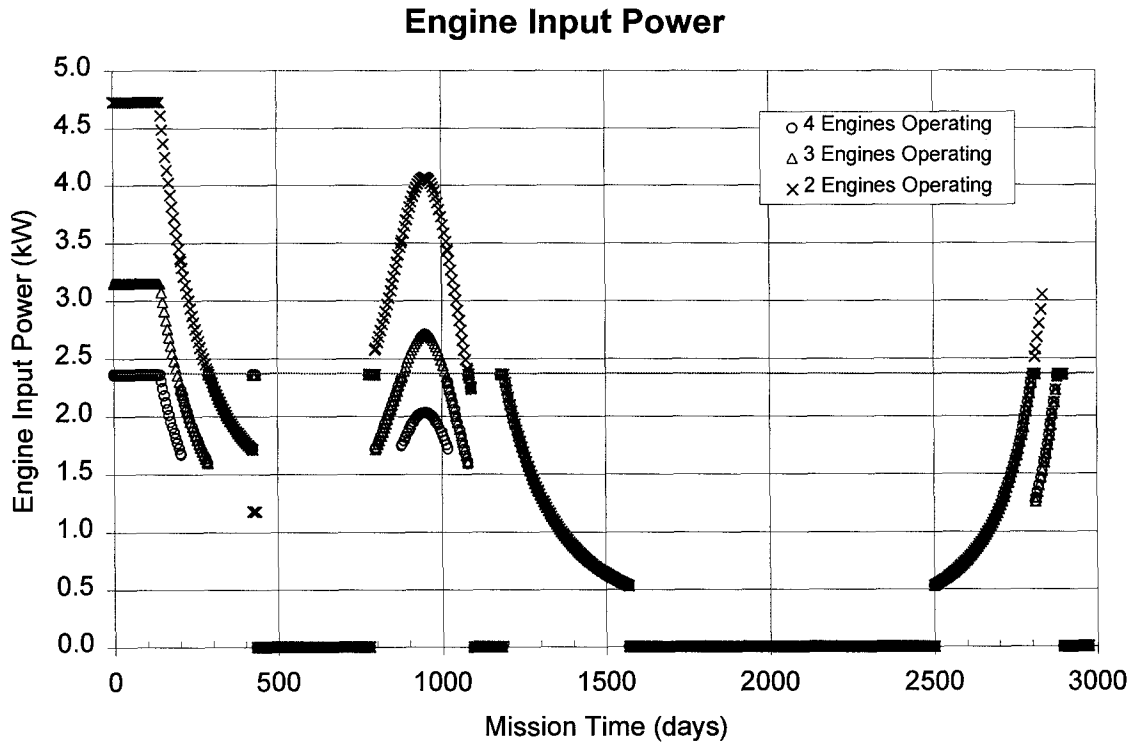


**Fig. 6 Engine input power variation during the CNSR mission.**

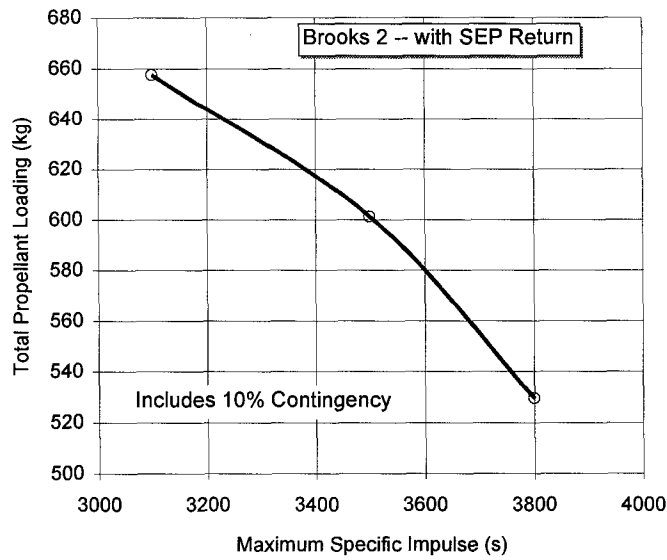


**Fig. 7 Increasing the maximum engine  $I_{sp}$  from 3100 s to 3800 s saves more than 100 kg of propellant for CNSR.**

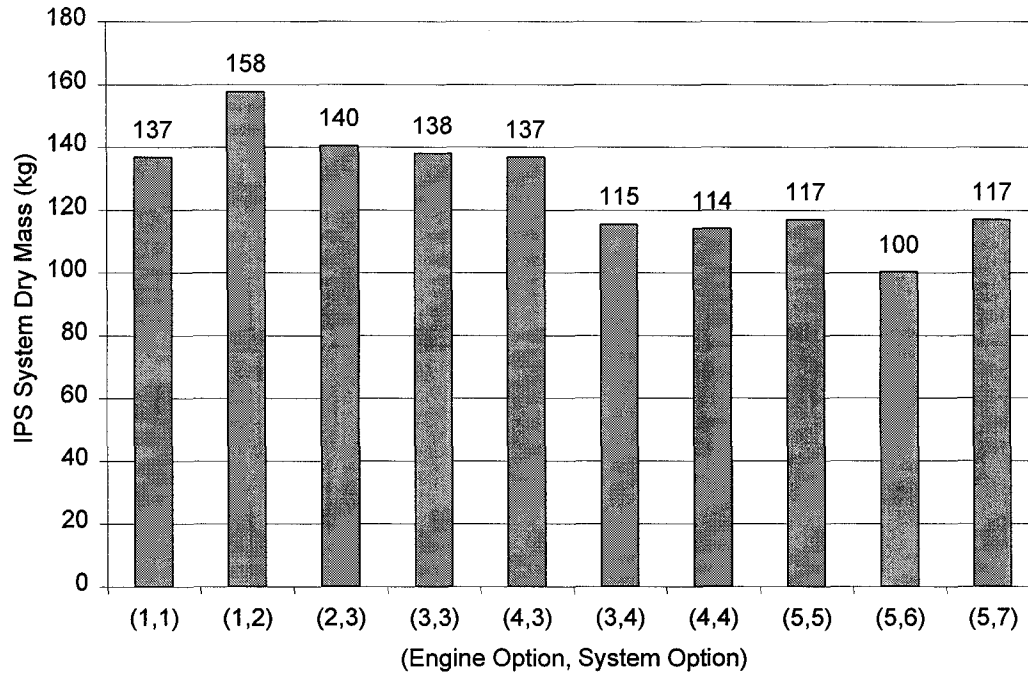


**Fig. 7 Ion propulsion system (IPS) dry mass indicates lighter system masses for more advanced technologies. Engine and system options are identified in Tables 3 and 4.**

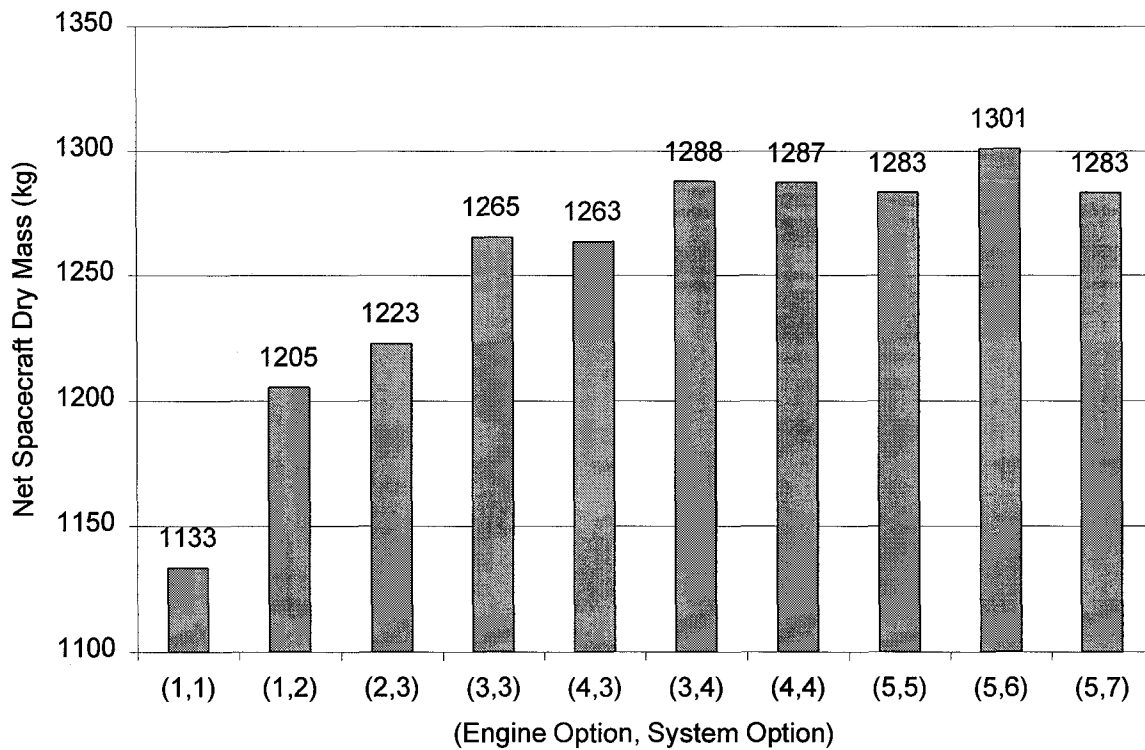


**Fig. 8 The net spacecraft dry mass is defined as the initial spacecraft wet mass minus the xenon propellant and the IPS dry mass. Larger net spacecraft masses are better. The largest net masses are obtained with the most advanced SEP technologies. The (engine, system) combination (4,3) offers the best combination of increased net spacecraft mass and low risk.**

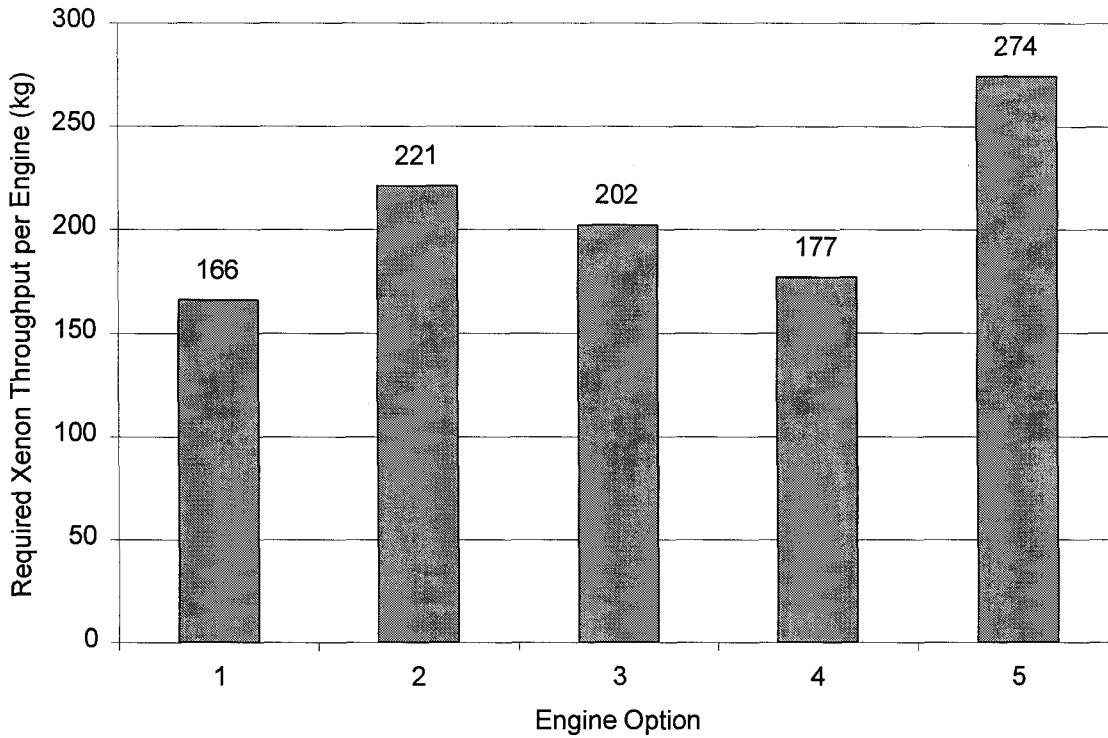


**Fig. 9** Required throughput per engine. Engine Option 1 assumes 4 engines are used to process the total propellant load. Engine Options 2, 3, and 4 assume only 3 engines are used, and Engine Option 5 assumes only 2 engines are available to process the required propellant load.

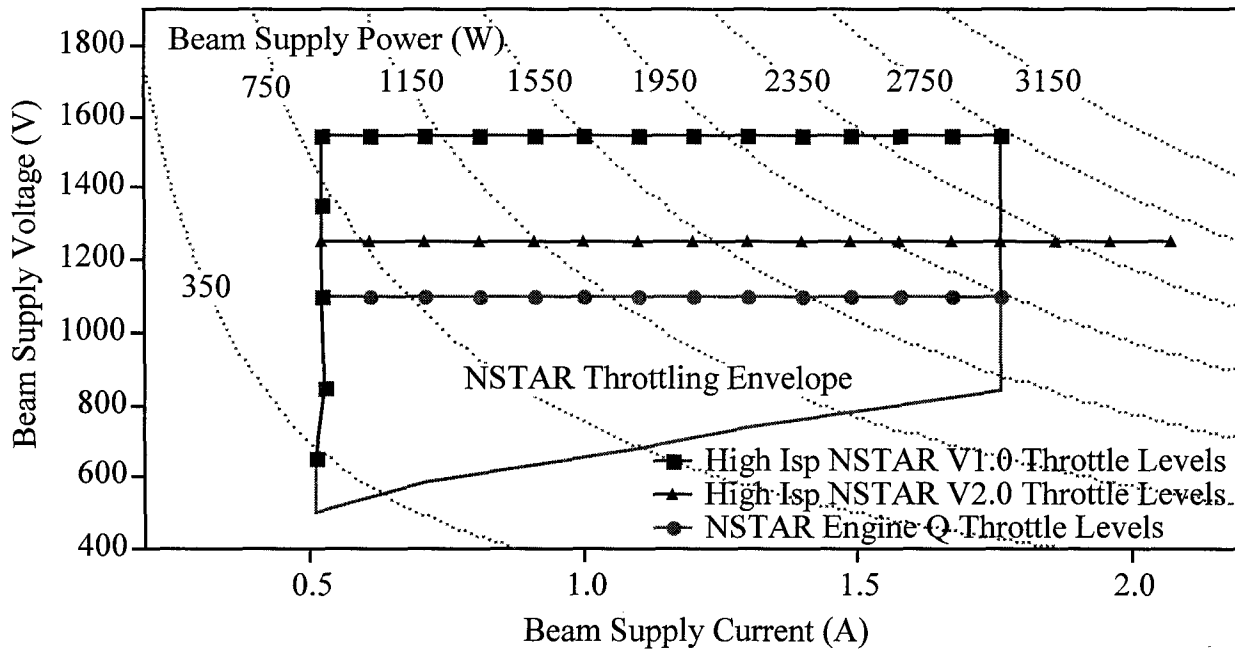


**Fig. 10** Throttling envelopes for Engine Options 1, 3 and 4. Engine Option 4 requires no increase in beam current beyond that demonstrated in the NSTAR project's extensive long-duration test program.

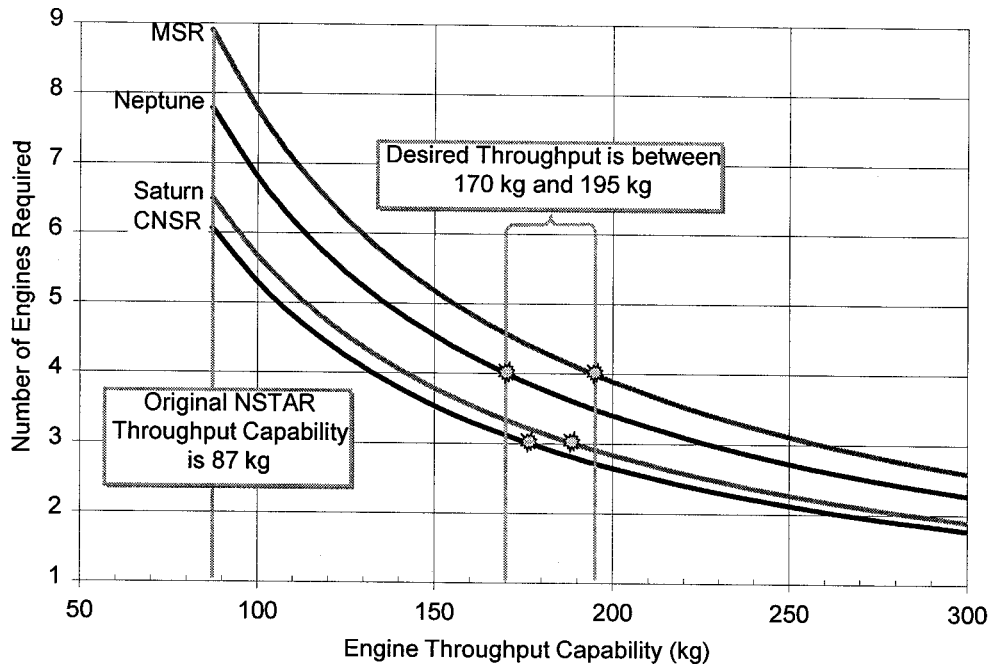


**Fig. 11** The number of engines required to process the total propellant load decreases significantly as the engine throughput capability increases.

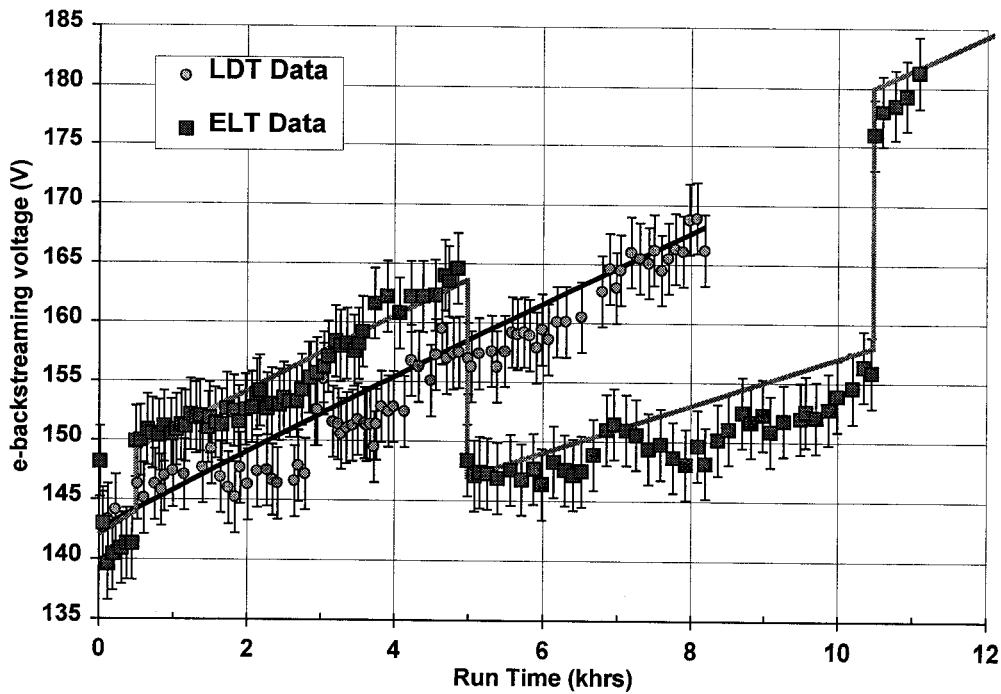


**Fig. 12** Electron-backstreaming variation with run time from the NSTAR project's two long-duration tests, the Life Demonstration Test (LDT), and the Extended Life Test (ELT). The solid line is a semi-empirical model used in the analysis of this failure mode.

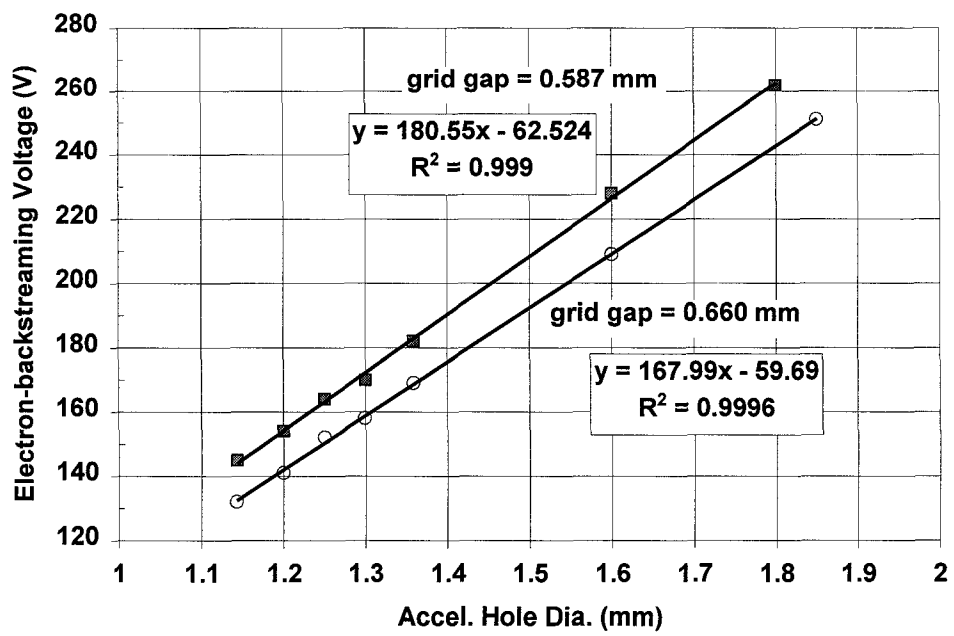


**Fig. 14** Calculated variation of electron-backstreaming voltage with hole diameter and grid separation.

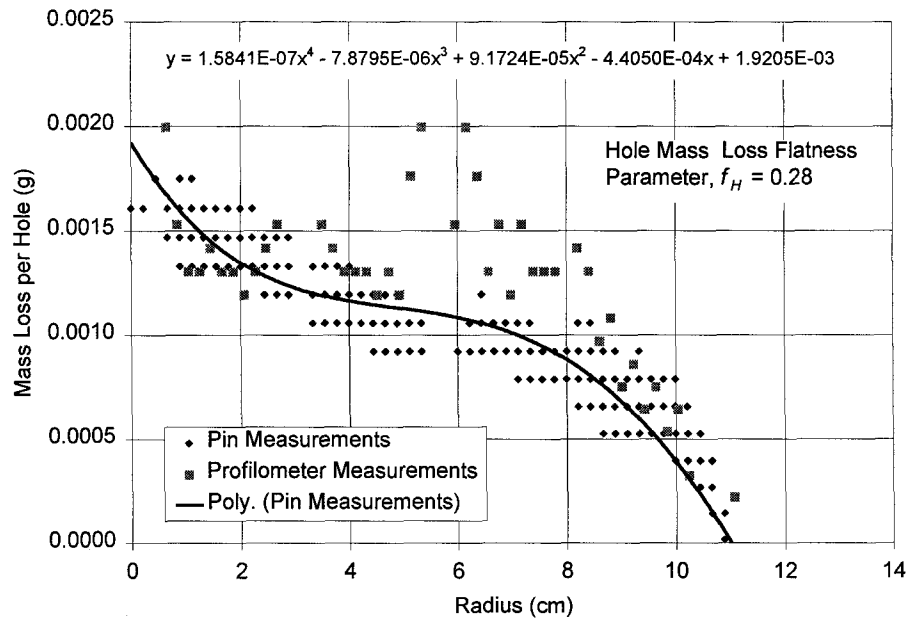


**Fig. 15** Hole mass loss profile used to calculate hole erosion flatness parameter.

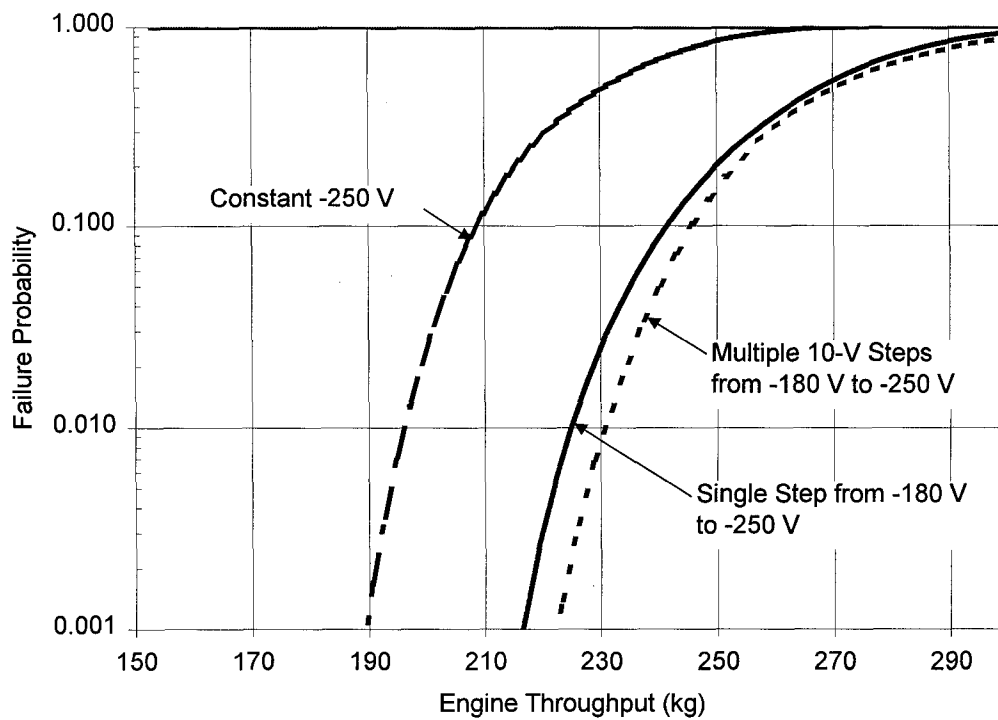


**Fig. 16** Accelerator grid wear-out failure probability due to grid erosion.